Calibration of GISSMO Model for Fracture Prediction of A Super High Formable Advanced High Strength Steel

Xiaoming Chen, Guofei Chen, Lu Huang, Ming F. Shi
United States Steel Corporation

Abstract

Advanced high strength steels (AHSS), due to their significantly higher strength than the conventional high strength steels, are increasingly used in the automotive industry to meet future safety and fuel economy requirements. Material failure that was rarely observed in crash tests a decade ago occurs more frequently in AHSS parts due to the relatively low ductility when compared to conventional steels. In computer aided engineering (CAE) crash analysis, a fracture model is often integrated in the simulations to predict the effects of material failure during crash events. In this paper, parameters of a fracture criterion are generated and calibrated for a Super High Formable (SHF) Steel with a minimum tensile strength of 1180 MPa (1180SHF). A generalized incremental stress state dependent damage model (GISSMO) in Software of LS-DYNA® is employed to evaluate the fracture predictability in the crash and forming simulations. The fracture strains of the 1180SHF steel are experimentally characterized under various deformation modes encompassing shear, uniaxial tension, bending, plane strain and balanced biaxial stretch conditions. The GISSMO parameters are determined and calibrated using fracture tests at these deformation modes for the 1180SHF steel. Validation simulations are performed on three-point bending component crash tests and good correlations are achieved. The validated GISSMO card for the 1180SHF steel can be used in CAE simulations of automotive structures.

Introduction

Advanced High Strength Steels (AHSS) have the advantages with high strength and improving crash energy absorption when compared to conventional steels. In recent years, AHSS have been widely accepted as the material of choice to balance vehicle weight, vehicle crash, durability and NVH performance. While the increased usage of AHSS resulted in weight savings, one performance parameter to be studied is fracture during a vehicle crash and some forming events. Fracture that was rarely observed in crash tests a decade ago occurs more frequently in AHSS parts due to the relatively low ductility when compared to conventional steels. To improve the AHSS ductility, a new high formable 1180 MPa steel grade, USS-1180SHF, which combines high strength and superior ductility is developed for automotive applications. The super high formability of 1180SHF presents a great opportunity to replace hot-stamped structural parts with similar mass savings at reduced costs and maintain the vehicle crash performance.

To appropriately apply AHSS and maximize weight reduction potential, it is important to develop the capability to predict the fracture behavior correctly in crash simulations and to accurately assess designs during the vehicle development process. Although crash simulations have been successfully used during vehicle development to assess the energy absorption capability of the vehicle, continuous improvements in many areas are still required to further improve the quality of the crash simulations. One of the areas is the prediction of the fracture behavior of structural components under different loadings. Crash simulations that do not take into account the fracture behavior may overstate the load-carrying capacity and the absorbed energy of a structural component. The application of AHSS fracture prediction becomes more important since those materials can be relatively prone to fracture during crash and forming deformation.

Several material models available in the widely used Finite Element Analysis (FEA) code LS-DYNA are adopted to simulate the fracture behavior of AHSS. For example, material model (MAT 123), *MAT_MODIFIED_ PIECEWISE_ LINEAR_PLASTICITY uses a major in-plane strain or the major principal

strain as the failure criterion. The modified Mohr-Coulomb (MMC) fracture model [1] with stress triaxiality dependent equivalent plastic strains as the failure criterion is also implemented (MAT 224). The applications of different material models for ductile fracture predictions can be found in automotive component analyses [2, 3]. The GISSMO material model provides additional features and flexibility for modeling the AHSS fracture behaviors [4-6]. In this study, the 1180SHF fracture behavior is investigated using the (MAT 24) *MAT_PIECEWISE_ LINEAR_PLASTICITY with the addition of *MAT_ADD_EROSION and GISSMO model. Model parameter calibrations were performed on the tests of uniaxial tension, shear, dome and V-bending. Validation simulation is also conducted on a three-point bending crash test. The predicted results are in good agreement with the test data.

GISSMO Model Review

GISSMO is a phenomenological ductile fracture criterion. The fracture strain limit curve, equivalent plastic strain versus stress triaxiality, under plane stress state $\varepsilon_f(\eta)$ can be determined by several experiments. The stress triaxiality ($\eta = \sigma_m / \sigma_v$) is defined as the ratio of mean stress over von Mises stress. In this study, test data are used to generate the fracture strain limit curve. The fracture strains of the 1180SHF were experimentally determined under four different strain conditions. Mini-shear test was conducted to obtain the fracture strain of 1180SHF under shear condition. Marciniak cup test was employed to evaluate its fracture strains under uniaxial tension, plane strain and balanced biaxial stretch conditions. Digital image correlation (DIC) technique was used for strain analysis. Supplementary thinning measurements were used to improve the measurement accuracy [7]. Detailed discussion on the test methods can be found in previous publications [6-10].

The fracture locus was determined by fitting the experimental data using the Hosford Coulomb fracture initiation model (Eq. 1) [10], as shown in Figure 1. The parameters (*a, b, c,* and *n*) of the model are determined as summarized in Table 1.

$$\bar{\varepsilon}_f(\eta) = b(1+c)^{\frac{1}{n}}\left\{\left[\frac{1}{2}\left[(f_1-f_2)^a+(f_2-f_3)^a+(f_1-f_3)^a\right]\right]^{\frac{1}{a}} + c(2\eta+f_1+f_3)\right\}^{-\frac{1}{n}} \quad (1)$$

With $f_1[\bar{\theta}\,] = \frac{2}{3}\cos[\frac{\pi}{6}(1-\bar{\theta}\,)]$, $f_2[\bar{\theta}\,] = \frac{2}{3}\cos[\frac{\pi}{6}(3+\bar{\theta}\,)]$, and $f_3[\bar{\theta}\,] = -\frac{2}{3}\cos[\frac{\pi}{6}(1+\bar{\theta}\,)]$

where $\bar{\theta}$ is the lode angle parameter*; a, b,* and *c* are material parameters; *n* is the work hardening exponent.

Table 1. Hosford Coulomb fracture initiation model parameters based on curve fitting to experimental data.

a	b	c	n
1.71	0.65	0.032	0.09

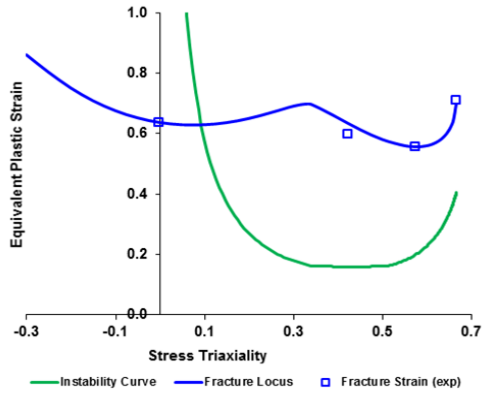

Figure 1. Experimental fracture strain data, fracture locus based on Hosford Coulomb fracture initiation model and instability curve.

Another curve is the instability curve, $\varepsilon_{crit}(\eta)$, defined as the equivalent plastic strain at the onset of diffuse necking. The curve is adjusted using the uniform elongation value tested from uniaxial tension. Figure 1 also shows the instability curve for the 1180SHF steel.

The damage accumulation rule is given by the equation:

$$\Delta D = \frac{N}{\varepsilon_f} D^{(1-\frac{1}{N})} \Delta\varepsilon_v \qquad (2)$$

where N is the damage exponent. The incremental damage ΔD, incremental plastic strain $\Delta\varepsilon_v$ is calculated at every time step. When the damage value D reaches 1.0, fracture initiates and the element is deleted. Accumulating in each time step, Equation (2) is suitable for fracture calculation during non-proportional strain paths.

The same rule is also used for calculating the accumulation for instability measure. When the instability measure accumulates to 1.0, coupling of damage to stress is started using the equation below:

$$\sigma^* = \sigma\left[1 - \left(\frac{D-D_{crit}}{1-D_{crit}}\right)^m\right] \qquad \text{for } D \geq D_{crit} \qquad (3)$$

Where D_{crit} is the threshold damage value at the time step when instability initiates; m is the fading exponent which is calibrated with test data. The 1180SHF steel possesses high post elongation and its fracture strain is sensitive to the parameter of stress fading out.

Another feature of the GISSMO model is mesh regularization which provides a solution for the element size effect on the strain calculation.

Calibration

The parameters for the GISSMO model are calibrated in LS-DYNA through the simulations of the uniaxial tension test, shear test, V-bend test and dome tests. The anisotropy for this material is not significant and therefore is not considered in the analyses. Fully integrated shell element (type 16) and von Mises yield criterion, i.e., *MAT_PIECEWISE_ LINEAR_PLASTICITY (MAT 24) are used in the simulations. The GISSMO model is implemented in LS-DYNA through the use of the keyword *MAT_ADD_EROSION. The calibration process and results are described in details below.

Stress-strain curves

Table 2 shows the tensile properties of the as received sheet at the thickness of 1.2 mm. The uniform elongation is 0.064 (true strain). Figure 2 shows the true stress-true plastic strain curve. Shear stress-strain curve can be obtained in the shear test. After converted to equivalent stress and strain, the stress and strain curve can be extended to true strain of 0.6. The curve is also shown in Figure 2. The curve is further extrapolated to true plastic strain of 1.0 using power law model. This curve is then used in the calibration in this study.

Table 2. Tensile properties of the USS-1180SHF steel.

Steel Grade	Yield Strength (MPa)	Tensile Strength (MPa)	Uniform Elongation (%)	Elongation (%)	n value	R
1180SHF	958	1219	0.09	14.8	0.09	0.94

Damage Accumulation Exponent N

Sensitivity study was conducted on the damage accumulation exponent *N* by simulating the uniaxial tension test. Damage rules with N=1 to 5 were compared in the simulations. Figure 3 shows little difference for the simulated Force vs Displacement curves when N=2 to 5. The results are in good agreement with experimental data. Therefore, it is assumed that the result is not sensitive to the damage exponent for this material, and the quadratic damage rule (N=2) is used in this study.

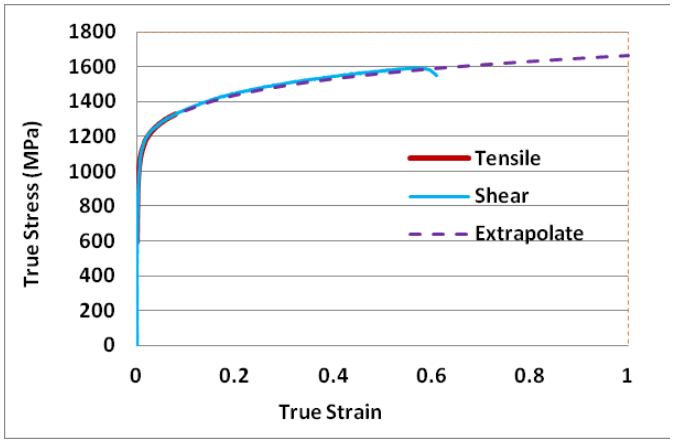

Figure 2. Stress-strain curve for the USS-1180SHF steel

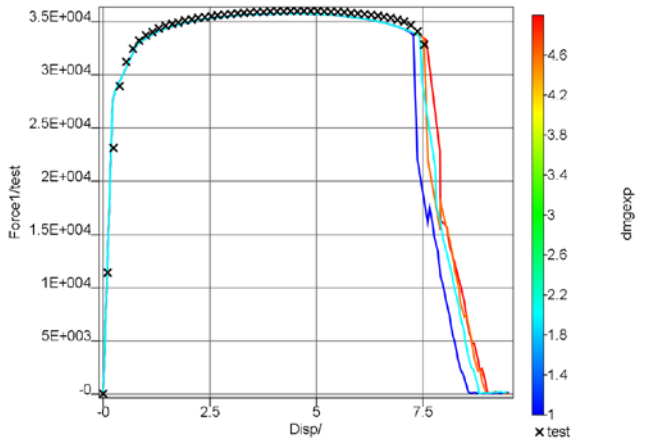

Figure 3. Effect of damage accumulation exponent on strains

Uniaxial Tension Test

Uniaxial tension test was used as a baseline model. The DIC method was used to measure the strain in the tests and the gage length of 0.5 mm was used for the fracture strain measurement. However, much larger element sizes are often used in full scale crash simulations and a scale factor for the fracture strain must be introduced for various element sizes. To use the test data for different element sizes, GISSMO model provides a mesh regularization feature. Both fading exponent and equivalent plastic strain to failure can be regularized with various element sizes. In this study, four element sizes, i.e., 0.5, 1.0, 2.5, and 5.0 mm, were used to cover the sizes from lab test to full scale model simulations. Eight parameters need to be determined in the calibration. The trial and error method to find the parameter values from a random range would be very time consuming. Optimization method is a very efficient way to find the proper parameters.

The optimization Software package of LS-OPT® was used in this study. The optimization objective is to match the experimental force-displacement curve with the simulation results of various element sizes. Numerous iterations were searched by LS-OPT and the results are shown in Figure 4 on different combinations. The optimized results are shown in Figure 5, where the solid lines are the curves of forces vs. displacements from simulations with different element sizes. There is little difference among the curves of different element sizes,

which shows the effectiveness of the mesh regularization. The simulation results are also in a good agreement with the test data which is shown as a cross-dot line. These parameters are best fit not only for tension tests but also for the other tests shown later.

To further validate the effectiveness of the mesh regularization, the optimized parameters were used to perform a single simulation on the tension test using four different element sizes. The predicted equivalent strain distribution at fracture is shown in Figure 6, in which the model is able to predict the failure for all 4 element sizes used in the model. A tested sample is also shown in Figure 6. Figure 7 shows the contour of stress triaxiality before necking in the samples, which is close to 0.33, i.e., the uniaxial tension stress state, for all four element sizes.

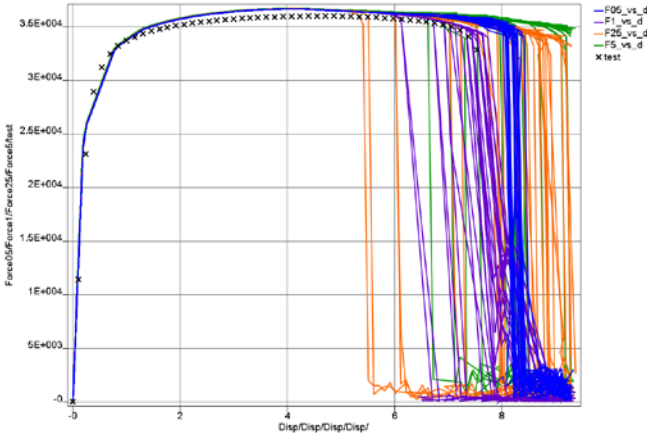

Figure 4. Simulation results at different iterations during optimization.

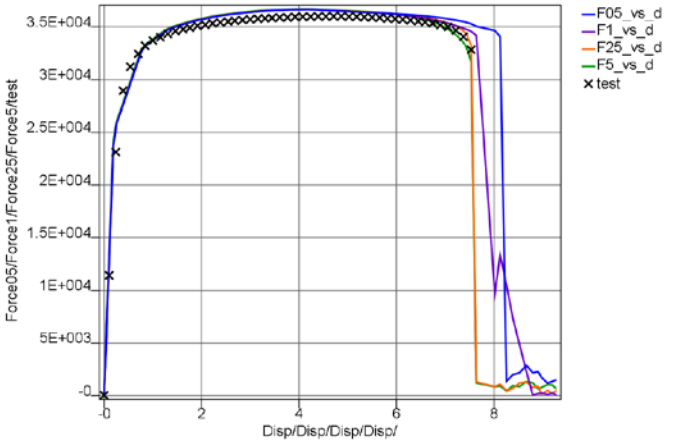

Figure 5. Simulated force-displacement curves at four mesh sizes using the optimized parameters.

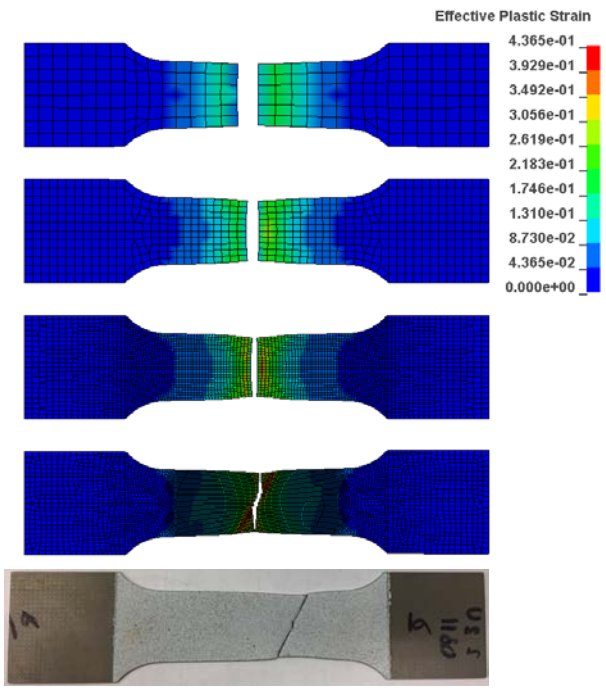

Figure 6. Predicted equivalent strain distributions at fracture and a tested sample.

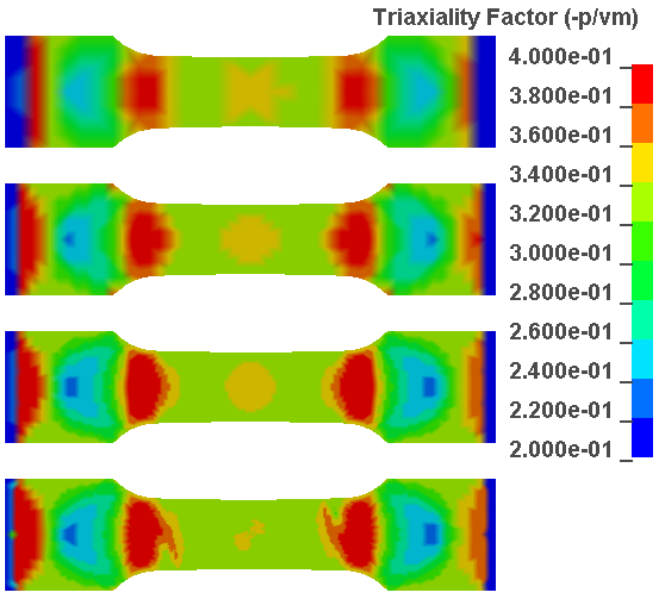

Figure 7. Stress triaxiality at different element sizes.

V-Bend Test

Similar analysis method from the tension sample test was used for the V-bend sample test calibration. Optimization was run to determine the best parameters. The objective is to match the force vs displacement curves from tests and the variables are the mesh size regularization scale factors and the stress fading exponents. The simulation force was obtained from the contact force between punch and specimen. Figure 11 depicts the FEA model for the V-bend test and the plastic strain distribution when fracture initiates. A tested sample is also shown. Figure 12 shows the simulation results. Since the contact setup may not perfectly match the test condition and simulated force may not perfectly fit the test data, the optimization result at the last iteration may not be the best one. The parameters corresponding to tension calibration were used and the comparison is shown in Figure 12. The simulation results are in a good agreement with the test data.

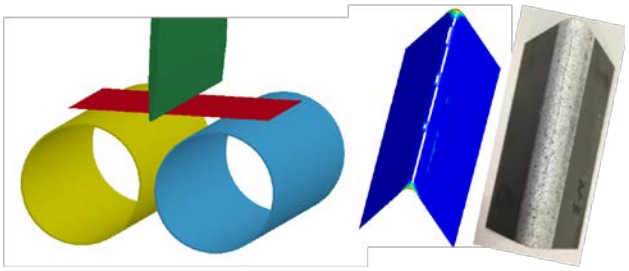

Figure 11. FEA model and a tested sample of the V-bend test.

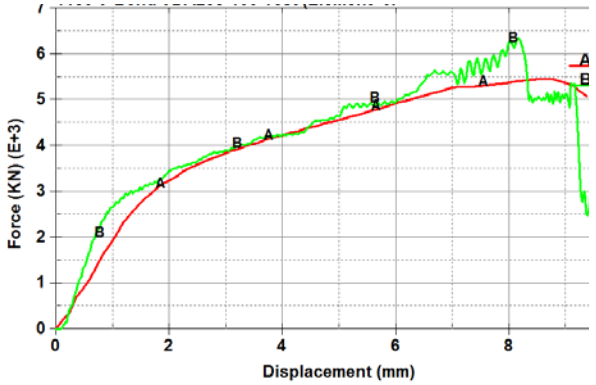

Figure 12. Simulations of the V-bend test at different

Shear Test

Optimization was also run to match the force-displacement curves between simulation and the shear tests. Figure 8 shows the comparison of the optimization result with the test data. The cross-dot line is the test result. The purple solid line is the final result of optimization simulations which is in a good agreement with the test data. Figure 9(a) shows a tested sample, (b) shows the fracture area and (c) shows the shear stress distributions before fracture. The maximum shear strain can be found in the elements in the center area of the specimen. The strain paths of those elements are closely along with the shear strain path as shown in Figure 10.

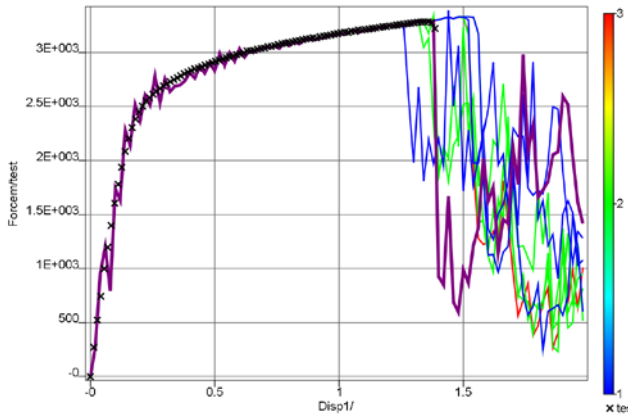

Figure 8. Simulations of the shear test at different iterations during optimization.

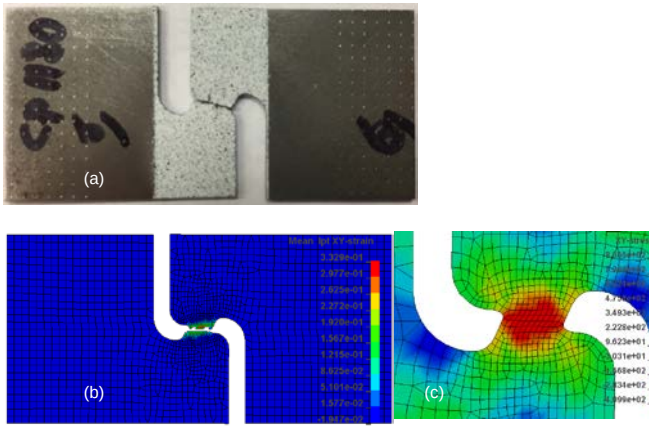

Figure 9. (a) A tested sample, (b) Fracture area and (c) The shear stress distributions before fracture

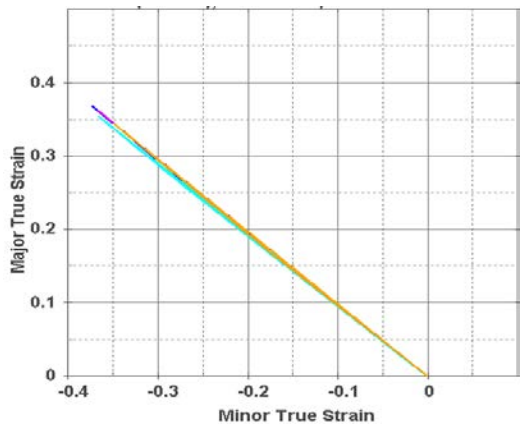

Figure 10. Strain path from simulation of the shear test.

Dome Tests

Dome tests were also simulated for parameter calibration. Three different blank geometries were used to generate different strain paths, i.e., uniaxial tension, plane strain and equal biaxial stretch. Figure 13 shows the FEA model for the plane strain case and Figure 14 shows the strain distributions at fracture and the tested samples for the three cases. The biaxial sample shows different fracture mode because an anisotropic material model is not used in the simulations.

Calibrations were carried out to match the force-displacement curves between the simulations and tests. The simulation forces were obtained from contact forces between punch and specimen. Due to the contact setup and dynamic effect, it is difficult to match the test force perfectly. Instead of matching the force, calibration was set to match the dome height at fracture. In the optimization run, the best result may not be the one in the last iteration. The best result was selected to fit the dome height at fracture. Figure 15(a) shows the simulation results for all the iterations. Figure 15(b) shows the biaxial stretch using parameters corresponding to tension calibration. The result is in a good agreement.

Figure 17 shows the stain paths for the three cases and they are closely along the strain paths of uniaxial tension, plane strain and equal biaxial stretch, respectively.

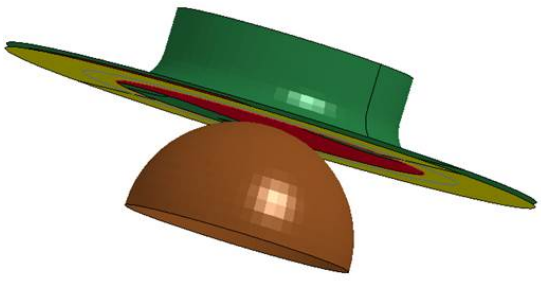

Figure 13. Dome tests with three different blank geometries.

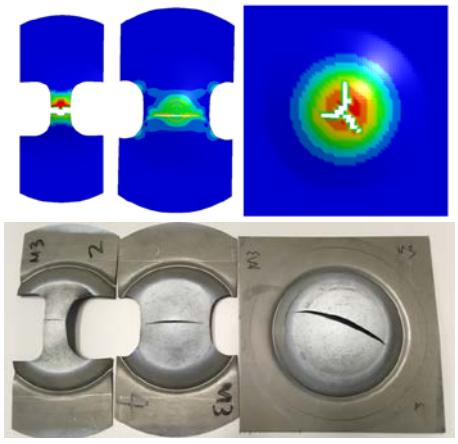

Figure 14. Dome tests with three different blank geometries.

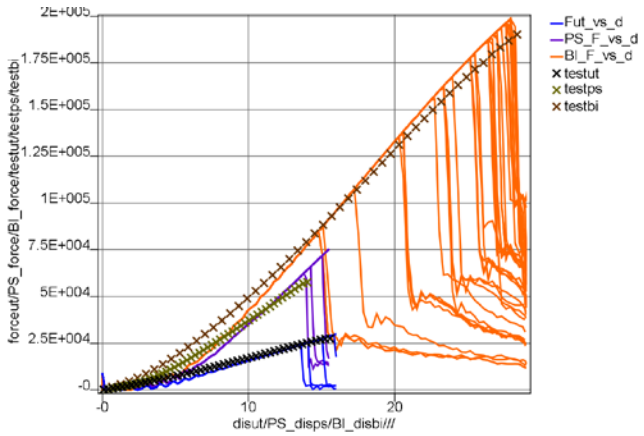

Figure 15. Simulations of the three dome tests at different iterations during optimization.

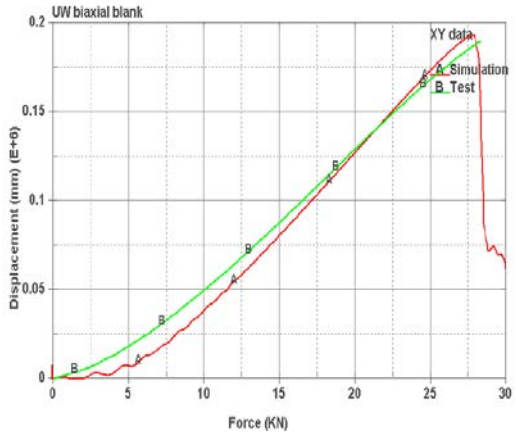

Figure 16. Result comparison for biaxial

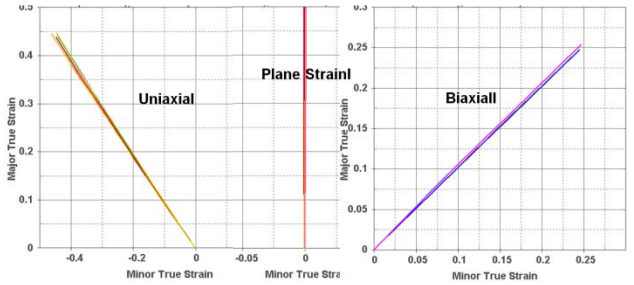

(a) Uniaxial tension (b) Plane strain (c) Biaxial stretch

Figure 17. Stain paths for the three dome tests.

Validation with Three-Point Bending Crash

The calibrated parameters, including mesh regularization factors and stress fading exponents, for all cases are shown in Figure 18. These parameters may not perfectly match all the test cases, but are the best fit data.
A three-point bending crash test at the crash velocity of 6.0 m/s was used to validate the calibrated parameters. The details of the three-point bending crash tests can be found in [12]. The stress-strain curves at various strain rates are shown in Figure 19. The crash test results with five replicates are shown in Figure 20 and the corresponding simulation model is shown in Figure 21(a). To capture the actual condition of the crash specimens, forming simulation result of the specimen with a hat section was included. High strain rate test data were also used in the simulation. Figure 21(b) shows the predicted fracture locations, which agree with the test results shown in Figure 20. Figure 22 compares the crash forces between simulations and tests. The simulation results with the calibrated GISSMO fracture model match the test results well. Comparing with the simulation results without a fracture model, it can be seen that the crash forces are similar at the displacement lower than 45 mm, but the force level for the simulation with the GISSMO fracture model is lower at the displacement larger than 45 mm, which indicates the fracture occurs after element deletion and the crash force drops.

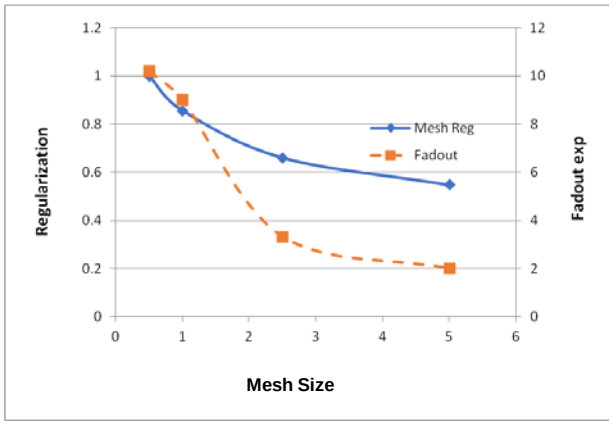

Figure 18. Mesh regularization and stress fading exponent after calibration.

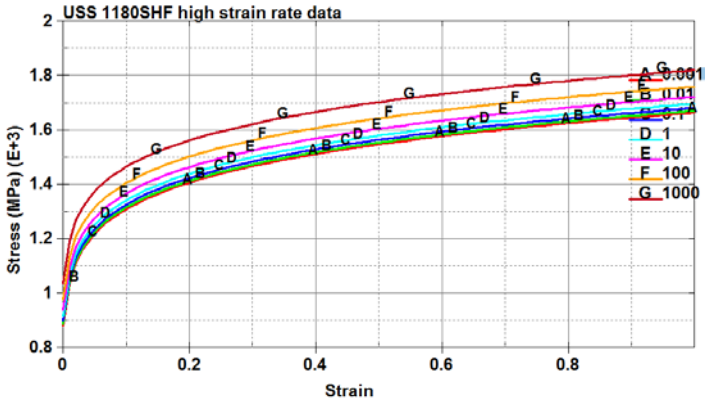

Figure 19. Stress-strain curves at high speed tests

Specimen	Maximum Load (kN)	Total Crack Length (mm)
1	33.0	146
2	31.1	143
3	31.4	140
4	32.8	139
5	33.3	141
Average	32.3	142

Figure 20. Three-point bending crash test results.

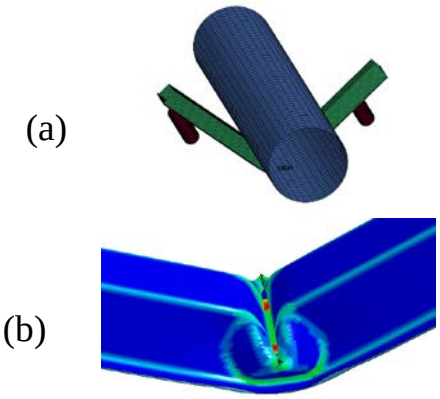

Figure 21. (a) Crash simulation model of the three-point bending test (b) Fracture prediction by the GISSMO model

Figure 23 compares the crash energy absorption vs. displacement between simulations and tests. Similar trend is observed again. The simulation results with the calibrated GISSMO model match well with the test data. Comparing with the simulation results without a fracture model, it can be seen that the curves are similar at the displacement lower than 45 mm, but the energy absorption reduces gradually to match the test results at displacement larger than 45 mm because facture is captured in the simulation with the GISSMO model.

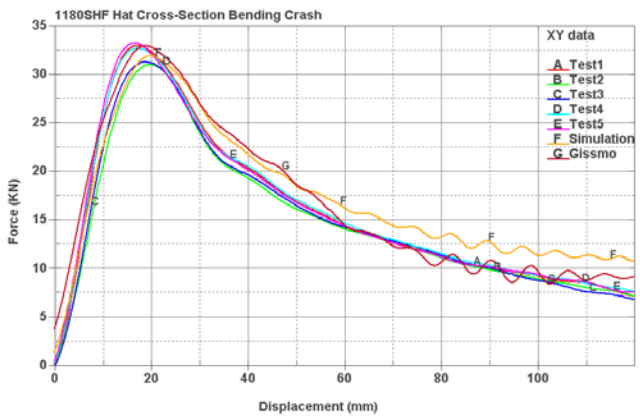

Figure 22. Comparisons of the crash force - displacement curves.

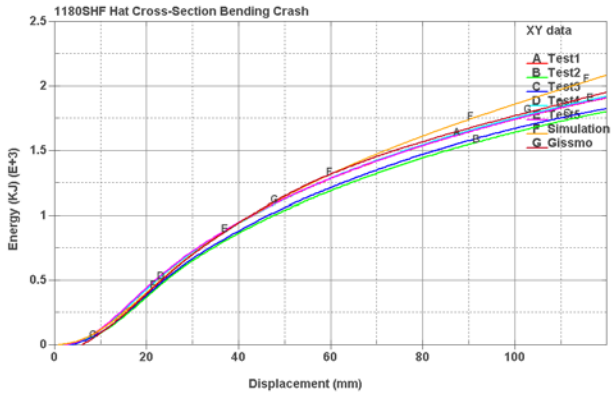

Figure 23. Comparisons of the energy absorption - displacement curves

Summary/Conclusions

- Parameter calibration of the GISSMO model for the USS-1180SHF steel has been performed using experimental data from the uniaxial tension, shear, V-bend and dome tests. The GISSMO model is validated with the three-point bending crash test.
- With the calibrated parameters, CAE simulation results are in good agreement with the uniaxial tension and shear tests, and reasonably good for the V-bend test.
- Calibrated parameters are validated in the simulation of a three-point bending crash test and good agreement is achieved.
- Optimization method with LS-OPT is an efficient way to find the proper parameters for the GISSMO model.

References

1. Y. Bai and T. Wierzbicki, "A New Model of Metal Plasticity and Fracture with Pressure and Lode Dependence," *Int. J. Plast.* 24 (6):1071-1096, 2008, doi:10.1016/j.ijplas.2007.09.004.
2. X. Chen, M. Luo, M. F. Shi, H. Shih, and T.Wierzbicki, "AHSS Shear Fracture Predictions Based on a Recently Developed Fracture Criterion," *SAE Int. J. Mater. Manuf.* 3(1):723-731, 2010, doi:10.4271/2010-01-0988.
3. G. Chen, M.F. Shi and T. Tyan, "Fracture Modeling of AHSS in Component Crush Tests", *SAE Int. J. Mater. Manuf.* 4(1):1-9, 2011, doi:10.4271/2011-01-0001.
4. J. Effelsberg, A. Haufe, M. Feucht, F. Neukamm, and P. Du Bois, "On parameter identification for the GISSMO damage model", *12th International LS-DYNA User Conference*.
5. F. Andrade, M. Feucht, and A. Haufe, "On the Prediction of Material Failure in LS-DYNA: A Comparison Between GISSMO and DIEM", *13th International LS-DYNA User Conference.*
6. X. Chen, G. Chen, L. Huang, "Validation of GISSMO Model for Fracture Prediction of a Third Generation Advanced High Strength Steel," SAE Technical Paper 2018-01-0107.
7. L. Huang, M.F. Shi, and P. Russell, "Determination of Fracture Strain of Advanced High Strength Steels Using Digital Image Correlation in Combination with Thinning Measurement," SAE Technical Paper 2017-01-0314, 2017, doi:10.4271/2017-01-0314.
8. A. Abedini, C. Butcher, D. Anderson, M. Worswick, and T. Skszek. "Fracture Characterization of Automotive Alloys in Shear Loading," *SAE Int. J. Mater. Manuf.* 8(3):774-782, 2015, doi:10.4271/2015-01-0528.
9. L.T. Kortenaar, "Failure Characterization of Hot Formed Boron Steels with Tailored Mechanical Properties." Master Thesis, University of Waterloo, 2016.
10. C. Butcher, "Experimental and Numerical Characterization of DP980 Steels for Forming and Crash Applications", Great Design in Steel seminar in May 2017.
11. G. Gu and D. Mohr. "Anisotropic Hosford–Coulomb fracture initiation model: Theory and application," *Eng. Fract. Mech.* 147 480-497, 2015, doi:10.1016/j.engfracmech.2015.08.004.
12. T.M. Link and B.M. Hance, "Axial and Bending Crash Performance of Advanced High-Strength Steels," AIST International Symposium on New Developments in Advanced High-Strength Sheet Steels, June 2017.

Acknowledgments

The authors would like to thank United States Steel Corporation for permission to publish this manuscript.

Disclaimer